The degradation mitigation effect of cerium oxide in polymer electrolyte membranes in extended fuel cell durability tests

Benjamin P. Pearman [a,b], Nahid Mohajeri [a,*], R. Paul Brooker [a], Marianne P. Rodgers [a], Darlene K. Slattery [a], Michael D. Hampton [b], David A. Cullen [c], Sudipta Seal [d]

[a] Florida Solar Energy Center, University of Central Florida, 1679 Clearlake Rd, Cocoa, FL 32922, USA
[b] Department of Chemistry, University of Central Florida, Orlando, FL 32816, USA
[c] Materials Science and Technology Division, Oak Ridge National Laboratory, Oak Ridge, TN 37831, USA
[d] Advanced Materials Processing and Analysis Center, Department of Mechanical Materials and Aerospace Engineering, University of Central Florida, Orlando, FL 32816, USA

HIGHLIGHTS

► Ceria nanoparticles incorporated into polymer electrolyte fuel cell membranes.
► Ceria decreases open-circuit voltage decay and fluoride emission in 94 h tests.
► Ceria decreases platinum deposition and broadens platinum band.
► Ceria remains effective over 500 h, resulting in almost no membrane degradation.

ARTICLE INFO

ABSTRACT

In this work, two formulations of cerium oxide nanoparticles were incorporated into perfluorosulfonic acid membrane electrode assemblies (MEAs) and their ability to improve the in-situ membrane durability was studied by subjecting them to 94 and 500 h open-circuit voltage hold accelerated durability tests. In the shorter test the open circuit voltage decay rate was reduced by half and the fluoride emission by at least one order of magnitude, though no effect on hydrogen crossover or performance on the baseline MEAs was measured. The presence of the additive increased the particle size but decreased the number of platinum catalyst particles that were deposited in the membrane. The main Pt band was found at the predicted location; however, the incorporation of ceria caused a broadening with particles reaching further into the membrane. In 500 h tests, ceria-containing MEAs demonstrated a seven-fold decrease in open-circuit voltage decay and three orders of magnitude reduction in fluoride emission rates with unchanged performance and hydrogen crossover, remaining effectively pristine whilst the baseline MEA underwent catastrophic failure.

© 2012 Elsevier B.V. All rights reserved.

1. Introduction

Polymer electrolyte membrane hydrogen fuel cells have the potential to become a large-scale source of clean stationary or portable electrical power, especially when combined with renewable energy production methods such as solar and wind. They are the leading technology able to provide a driving experience that is comparable, in terms of range and refueling behavior, to vehicles equipped with internal combustion engines. Currently, no membrane is able to withstand the harsh conditions of a hydrogen fuel cell environment for the more than 5000 h in automotive applications that are required for commercialization. Mechanical stresses such as swelling due to changes in relative humidity, differential gas pressures and compression combined with chemical attack cause membranes to degrade to such an extent that the cell fails [1].

The mechanisms of perfluorosulfonic acid (PFSA) ionomer chemical degradation are still the focus of much debate, however, there is a general consensus that reactive oxygen species such as hydroxyl or hydroperoxyl radicals are the main reagents. They are thought to form either directly in a reaction between hydrogen and oxygen on platinum or from hydrogen peroxide, which is formed at the electrodes, decomposition with metal impurities in the fuel cell [2]. These radicals attack vulnerable groups of the PFSA polymer, degrading the membrane [1,3–7].

Due to the large time scales involved in testing cells in real life conditions, accelerated durability test protocols have been developed [1]. In the open circuit voltage (OCV) hold test, cells are exposed to hydrogen and air or oxygen at low relative humidity (<50% RH) and open-circuit voltage, sometimes under pressure. At OCV conditions, insignificant amounts of the reactants are consumed and the gas crossover is maximized, leading to maximum production of radicals [8]. Consequently, the OCV hold test is often used as a method for specifically testing membrane degradation and the 500 h test protocol that is employed in this study has been established by the Department of Energy.

Several methods have been employed to reduce membrane degradation, including development of chemically stabilized membranes [9,10], mechanically reinforced membranes [11–16], alternate electrode materials [17–19] and the incorporation of hydrogen peroxide decomposition [11,12,20,21] or radical scavenging materials [6,21–33]. The latter approach is utilized in this research.

One of the most researched radical scavenging materials is the Ce(III)/Ce(IV) redox couple. This lanthanide is able to facilely switch between its two oxidation states, allowing it to quench radicals by donation or acceptance of electrons. The quenching reaction of HO$^{\bullet}$ by the Ce^{3+} ion is given in Eq. (1). Cerium oxide also known as ceria can act catalytically by returning to its Ce(IV) oxidation state through reaction with hydrogen peroxide, as shown in Eq. (2), or the hydroperoxyl radical, as shown in Eq. (3) [25,34]. In ceria, the cerium ions retain this radical scavenging behavior while bound in their oxide lattice. The ability of ceria to scavenge radicals is well known, especially in biological and medical applications [35–39].

$$Ce^{3+} + HO^{\bullet} + H^+ \rightarrow Ce^{4+} + H_2O \tag{1}$$

$$Ce^{4+} + H_2O_2 \rightarrow Ce^{3+} + HOO^{\bullet} + H^+ \tag{2}$$

$$Ce^{4+} + HOO^{\bullet} \rightarrow Ce^{3+} + O_2 + H^+ \tag{3}$$

In fuel cells, ion-exchanged PSFA membranes with low concentrations of Ce^{3+} ions have shown a 1000-fold reduction in fluoride emission rate (FER) over 200 h in OCV hold tests [34]. As a result of the ion-exchange, a noticeable reduction in performance and proton conductivity was measured. In order to avoid this detrimental effect, cerium oxide was added to recast membranes and was found to reduce FER by one order of magnitude without impacting performance over a 24 h test. This durability improvement was observed to be independent of nanoparticle concentration and formulation [25]. In a comparable work by Xiao et al., the OCV decay rate was found to be on the order of 0.1 mV h^{-1} for a 150 h OCV hold test, a sixty-fold reduction compared to a baseline MEA [6].

Most of the testing reported in the literature was short in duration. As a result, the ability of ceria to act catalytically over longer periods of time (hundreds of hours in accelerated tests) needs to be established. Furthermore, as a redox-active material, ceria can affect the potential profile present due to crossover hydrogen and oxygen. Its effect on the deposition of Pt catalyst within the membrane has not been determined. This work focuses on both long term degradation studies and ceria's effect on Pt band formation.

2. Experimental

2.1. Materials preparation

Nanoparticular ceria was prepared by thermal hydrolysis. Ammonium hydroxide, 0.50 ml, (Fisher Scientific; 29.04%) was added to 50 ml of a boiling solution of 0.02 M ammonium cerium nitrate (Acros Organics; 99.5% for analysis) in ethanol (Decon Labs;

200 proof) which, after the addition, was left to cool overnight under constant stirring. The yellow precipitate of cerium oxide that formed was centrifuged, washed five times with 5 ml of ethanol and then dried at 100 °C under vacuum, yielding ca. 0.17 g of product with particle sizes in 2–5 nm range.

The synthesized ceria was dispersed in ethanol in a Branson 2510 ultrasound bath using sonication at 40 kHz to give 7 mM colloidal dispersions in ethanol. Using the same technique, 7 mM dispersions of a commercial cerium oxide powder (Alfa Aesar; 99.9% min (REO), 20–150 nm) in ethanol were also prepared.

PFSA membranes were cast onto a porous PTFE support (Donaldson Filtration Solution; Tetratex® membrane; 7 μm) from solutions of 5% 1100 EW PFSA dispersions in alcohols (Ion Power, Inc.), ethanol and dimethylformamide (Acros Organics; 99.5% for HPLC) in a 5.8:4.0:1.0 volume ratio. Ceria was incorporated by replacing some of the ethanol with appropriate amounts of the ethanol dispersions to yield 0.5, 1.0 and 2.0 weight percent of cerium oxide relative to the polymer mass. Membranes without ceria were also cast as baselines. After room temperature drying, membranes were heated at 150 °C for 3 h under vacuum after purging three times with UHP nitrogen to remove all residual solvent.

2.2. Membrane electrode assembly fabrication (MEA)

A homogenized dispersion of a platinum on carbon powder (Tanaka; 46.7% Pt on C) in a methanol (Acros Organics; 99.9% for HPLC), deionized water and 5% 1100 EW PFSA in alcohol (Ion Power, Inc.) mixture was sprayed onto the membranes to give 25 cm^2 catalyst coated membranes (CCMs). Catalyst loadings were determined gravimetrically and kept at 0.375 ± 0.025 gPt cm^{-2}. The CCMs were ion-exchanged with cesium ions by immersing in a 0.05 M CsCO$_3$ (Alfa Aesar; 99% (metals basis)) solution overnight, followed by a 5 min hot press at 180 °C and then reprotonated by immersion in 0.5 M H$_2$SO$_4$ (BDH; 95.0%). The CCMs were built into 25 cm^2 hardware (Fuel Cell Technologies) with gas-diffusion layers (GDL) purchased from Ion Power, Inc. (Sigracet 10BC).

2.3. Single cell evaluation

2.3.1. Initial cell integrity tests

Internal and external leak tests were performed at room temperature. The absence of cell shorts was verified using a multimeter.

Table 1
List of MEAs and OCV hold conditions.

MEA	Ceria	# of cells
94 h OCV hold		
Baseline	None	3
Synthesized ceria	0.5 wt%	2
Synthesized ceria	1.0 wt%	2
Synthesized ceria	2.0 wt%	2
Commercial ceria	0.5 wt%	2
Commercial ceria	1.0 wt%	2
Commercial ceria	2.0 wt%	2
500 h OCV hold		
Baseline	None	1
Synthesized ceria	1.0 wt%	1
Commercial ceria	1.0 wt%	1

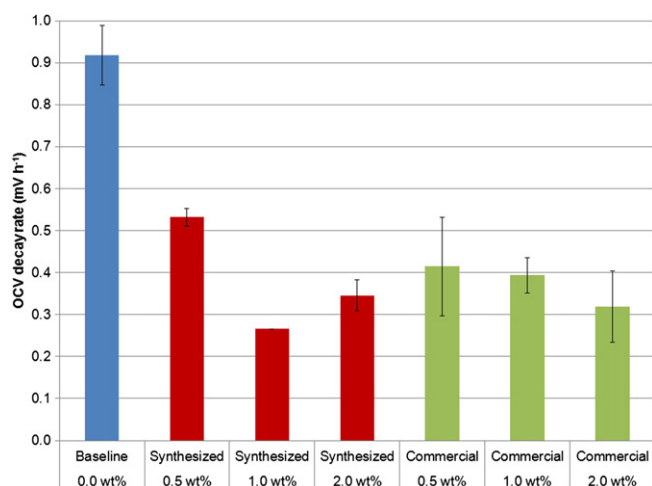| OCV hold test conditions	Type	Flow	RH	Pressure
94 h OCV hold anode fuel	H$_2$	200 cm^3 min^{-1}	30%	Ambient
94 h OCV hold cathode fuel	Air	200 cm^3 min^{-1}	30%	Ambient
500 h OCV hold anode fuel	H$_2$	350 cm^3 min^{-1}	30%	150 kPa
500 h OCV hold cathode fuel	Air	830 cm^3 min^{-1}	30%	150 kPa

Fig. 1. Average OCV decay rate of MEAs in 94 h OCV hold test.

2.3.2. Hydrogen crossover and platinum electrochemically active area measurement

Linear sweep voltammetry (LSV) was performed using a Princeton Applied Research Potentiostat/Galvanostat Model 263A at a cell temperature of 25 °C, anode saturator temperature of 25 °C and cathode saturator temperature of 25 °C (nomenclature of 25/25/25) with the anode gas of H_2 and cathode gas of N_2 (nomenclature of H_2/N_2) with flow rates of 170 cm^3 min^{-1} from 0.1 to 0.8 V at a sweep rate of 4 mV s^{-1}. Hydrogen crossover was calculated as the current density at 0.4 V.

Cyclic voltammetry (CV) was performed using a Princeton Applied Research Potentiostat/Galvanostat Model 263A at the same conditions as the LSV measurements between 0.025 and 0.8 V at 30 mV s^{-1} for five cycles. The electrochemically active area (ECA) of the platinum catalyst was calculated from the hydrogen adsorption area during the cathodic sweep.

These electrochemical measurements were performed using CorrWare software. Fuel cell testing was controlled and monitored using Fuel Cell software.

2.3.3. Cell conditioning

Cells were humidified by exposure to H_2/N_2 at 80/80/73 for 3 h and conditioned by running at benign fuel cell operating conditions of 0.55 V at 80/80/73 with H_2/Air for 3 h.

2.3.4. Cell performance

Performance was determined by obtaining polarization curves with both H_2/Air and H_2/O_2 at 80/80/73 on a Scribner 850C or a Teledyne Energy Systems, Inc. Medusa fuel cell test station.

2.4. Accelerated durability testing

In a 94 h OCV hold test, sets of eight cells were simultaneously exposed to OCV conditions at 90 °C with gas conditions listed in Table 1 on a Scribner Inc. Membrane Electrode Assembly Durability Test System (MEADS). LSV and CV measurements were performed before conditioning, before performance testing, and after the OCV hold.

In a 500 h OCV hold test, single cells were simultaneously exposed to OCV conditions with 90 °C with gas conditions listed in Table 1 on a Scribner 850C fuel cell test system. LSV and CV
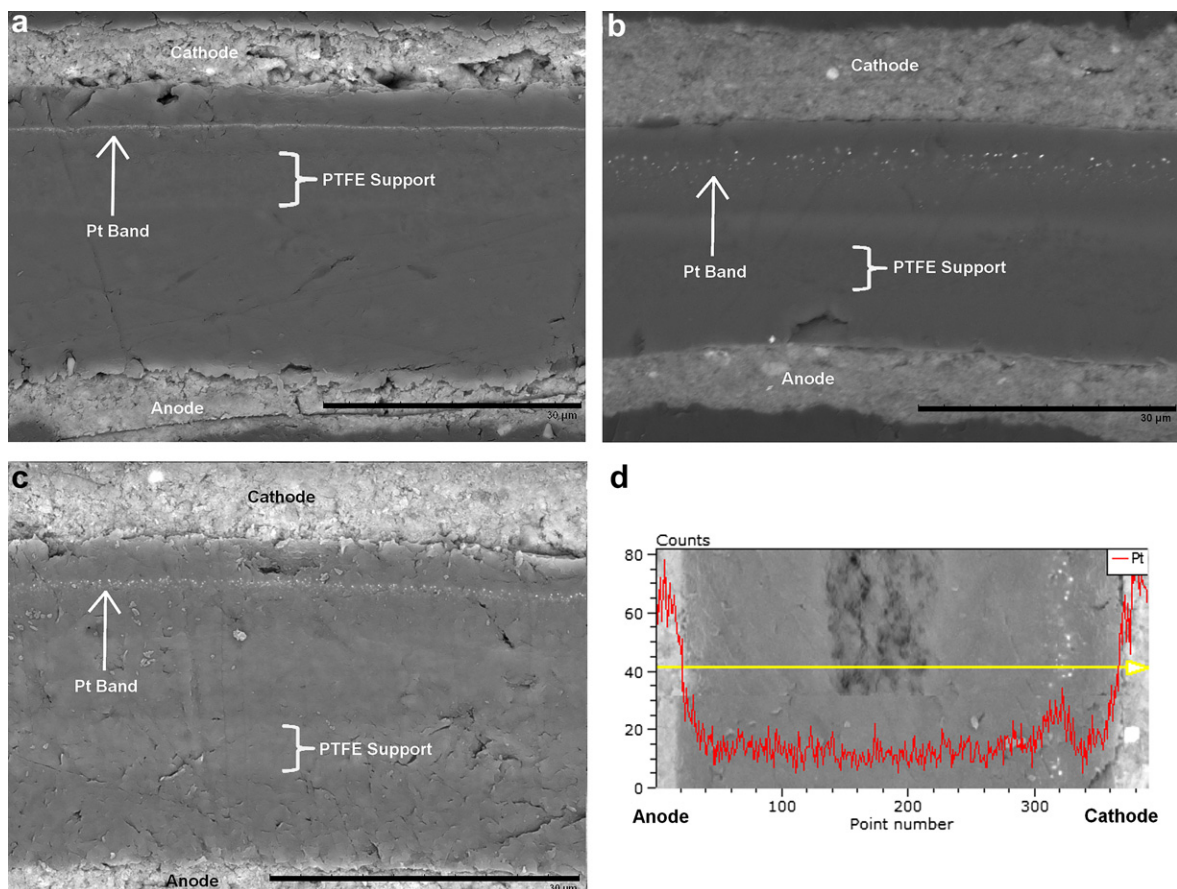

Fig. 2. SEM images of 94 h OCV hold tested CCM cross-sections: a) Baseline, b) synthesized ceria 2.0 wt%, c) commercial ceria 2.0 wt% and d) baseline with platinum EDS spectrum overlay.

measurements were performed before conditioning and before performance testing as well as every 24 h during the OCV hold. Additionally, the cell resistance and high frequency resistance (HFR) were measured daily, the former by holding the cell at 0.5 V at 90/61/61 under N_2/N_2 and the latter by holding the cell at 0.2 A cm^{-2} at 90/61/61 under H_2/air.

The MEAs measured are given in Table 1.

The OCV was monitored and water condensates were collected twice daily for the 94 h and once daily for the 500 h test and measured for fluoride ion content using ion chromatography on a Dionex ICS-1500 instrument equipped with AS9-HC carbonate eluent anion-exchange column.

2.5. Post-test imaging

Infrared (IR) images of tested CCMs were obtained using a Fluke Ti25 IR camera. The CCMs with gaskets were placed on a graphite plate and secured so that the cathode side was visible and exposed to air. A mixture of 4% hydrogen in nitrogen gas was allowed to flow on the anode side and IR images were recorded. Hydrogen gas that penetrated the membrane reacted with oxygen at cathode and the resultant exothermic reactions appeared on IR images as areas of elevated temperature.

A JEOL 2200FS instrument was used for high resolution scanning transmission electron microscopy, (S)TEM, imaging. Cross-sections of CCMs were prepared for imaging by embedding in Araldite 502 resin followed by microtoming to a thickness of approximately 75 nm using a Leica UC7 microtome. For scanning electron microscopy (SEM) imaging, membranes were embedded in resin (Struers; SpeciFix® Resin), polished and sputter-coated with gold. Imaging was performed on a Zeiss ULTRA-55 FEG SEM and Hitachi TM3000 SEM with an integrated energy-dispersive X-ray spectroscopy (EDS) Physical Electronics 5400 sensor.

Platinum particle counting and analysis was performed using ImageJ and Microsoft Excel software.

3. Results & discussion

3.1. 94 h OCV hold durability testing

3.1.1. Hydrogen crossover, platinum ECA, and performance

Two fuel cells with MEAs containing ceria concentrations of 0.5, 1.0 and 2.0 wt% for each ceria formulation, as well as three baselines, were built and tested.

The hydrogen crossover, determined with linear sweep voltammetry, was found to be below 1 mA cm^{-2} for all cells and did not change significantly after the 94 h OCV hold testing. The ECA of the catalyst was found to be around 65 cm^2 Pt gPt^{-1} and decreased during testing for all cells. This loss of active platinum is considered to be due to particle sintering, crystallite migration or dissolution [40–42]. No trends were observed with regards to the ECA due to ceria. The addition of ceria to the membranes had no significant
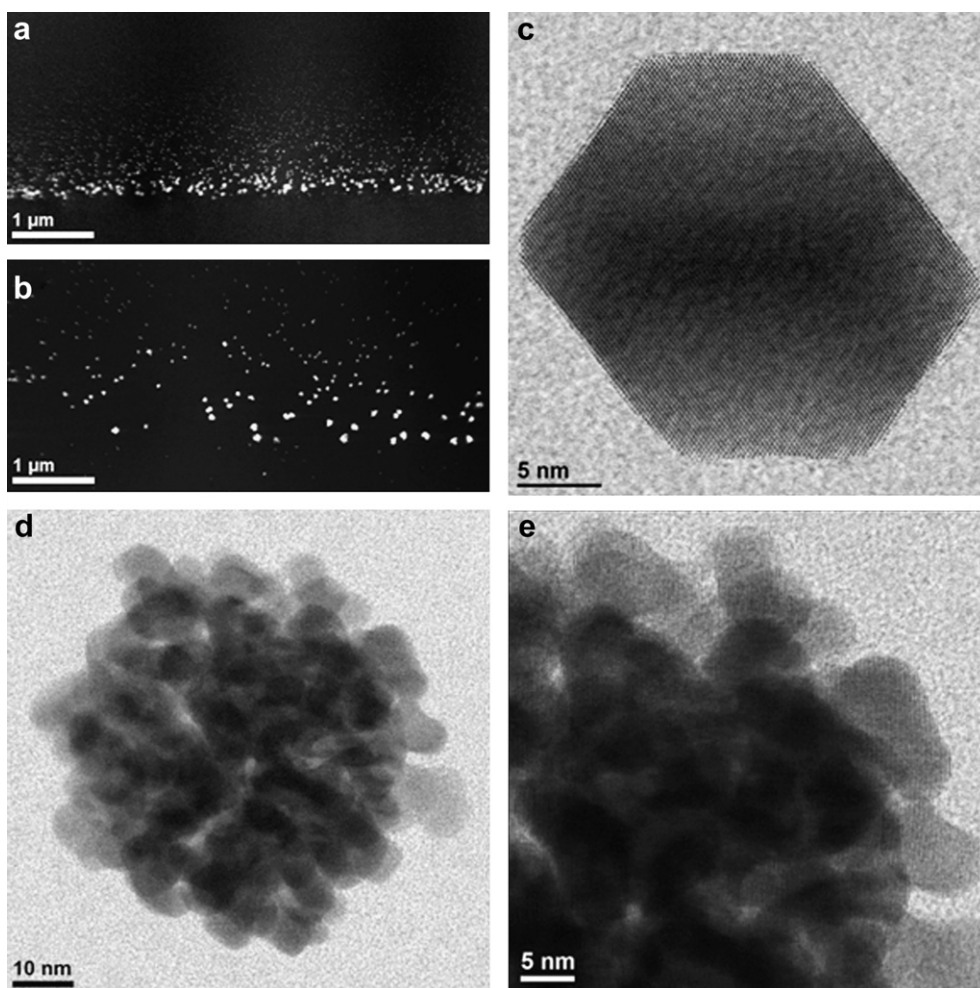

Fig. 3. STEM images of cross-sections of 94 h OCV hold tested MEAs: a) Pt band in a baseline MEA (cathode at bottom of image), b) Pt band in a commercial 1.0 wt% MEA (cathode at bottom of image), c) high magnification image of a faceted Pt particle, d) a dendritic Pt particle and e) high magnification image of a dendritic Pt particle.

effect on either the starting OCV or the performance of the respective cells, an observation confirmed by Trogadas et al. [25]. However, Xiao et al. [20] arrived at the conclusion that the addition of ceria negatively impacted the performance. Our group has observed slight variations in performance on a cell to cell basis, thought to be due to inhomogeneities in the manufacturing process. Within this error, no significant impact on performance was determined. The fact that neither the resistance nor the performance of any ceria-containing MEAs changed indicated that, under OCV hold conditions, ceria was not ionized but remained in its oxide lattice form, thereby not inhibiting proton transport.

3.1.2. OCV decay and fluoride emission

Fig. 1 shows the OCV decay rate of the cells over 94 h as a function of the ceria concentration in the membranes. The addition of ceria reduced the decay rate by approximately 50% compared to the baseline, though changes in the concentration of ceria had no significant effect. Further, the OCV decay rate mitigation was independent of additive formulation, and therefore, particle size.

While the baseline cells lost between 6% and 18% of their fluorine content, the fluoride ions released from the MEAs containing ceria were found to be below 1 ppm, which was the limit of quantification (LOQ) of the ion chromatograph used. Based on the LOQ, the ceria-containing MEAs lost less than 0.5% of their fluorine inventory, meaning that the addition of ceria reduced the fluoride emission rate by at least one order of magnitude with respect to the baseline MEAs. This confirms that the findings by Trogadas et al. [25] made in a 24 h test hold true even over longer periods of times.

SEM images of cross-sections, as given in Fig. 2a−c, showed no significant change in membrane thickness and IR images did not reveal any noticeable pinholes (not shown). For the time period measured, significant membrane degradation occurred in the baseline MEAs while the ceria-containing MEAs were comparatively unaffected.

3.1.3. Pt band formation

Fig. 2a−c show representative SEM images of cross-sections of MEAs demonstrating the formation of a distinct band of particles in the membrane. The nature of these particles, found at a distance of 3.5−4.5 μm from the cathode, was confirmed by EDS analysis (Fig. 2d) to be platinum.

It is known that during fuel cell operation, Pt is oxidized and dissolved from the cathode due to high potentials [43−45]. These dissolved ions migrate down a potential gradient towards the anode, and are reduced in the membrane by crossover hydrogen. As more and more of the catalyst precipitates, a band of Pt nanoparticles is formed. The distance of this band from the cathode has been found to be a function of the hydrogen and oxygen partial pressures [40,46−49]. The effect that the Pt band has on membrane degradation is still a matter of much debate. Some groups have shown increased degradation near the Pt precipitation [50,51]. Using a catalyst of platinum−cobalt on carbon, Rodgers et al. [52] found that Pt deposited evenly throughout the membrane rather than forming a distinct band. Though they provided no explanation for the origin of this effect, they observed that the fluoride emission was drastically lower than with a Pt/C catalyst. Others, however,
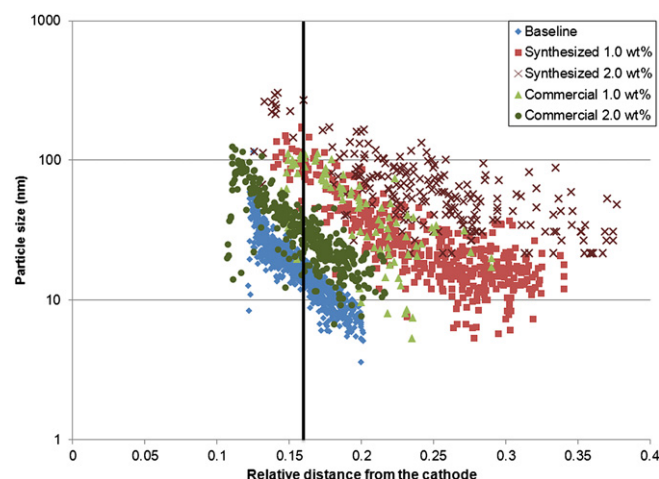

Fig. 4. Particle size as a function of normalized distance from the cathode (black line indicates the theoretical location of Pt band, based on references [58] and [59]).

have disputed the role of Pt in membrane degradation [53] and the addition of Pt particles has even been shown to increase durability [24,27]. A model proposed by Gummala et al. [54] suggests that the size and distribution of these platinum particles influences whether they have a significant detrimental impact on membrane durability.

Reports of Pt band particles in the literature have shown that they can be either faceted or dendritic, though the precise mechanism of growth is not well known [43,55]. We observed both structures, sometimes even within the same sample. Representative high magnification images of faceted and dendritic particles are given Fig. 3c and d, respectively, showing the crystal structure of both.

The inclusion of ceria into membranes had no effect on the types of Pt particles formed. However, SEM (Fig. 2) and TEM images (Fig. 3a and b) indicated that fewer particles were present in ceria-containing MEAs. Size and distribution of the Pt particles were determined from STEM images for five MEAs: a baseline, a synthesized ceria with 1.0 wt% and 2.0 wt% and a commercial ceria with 1.0 wt% and 2.0 wt%.

As listed in Table 2, the average Pt particle size for the baseline MEA was two to four times smaller than for the ceria-containing MEAs, though it should be noted that there was a significant variation in particle size within each sample. Fig. 3a and b clearly show the fading of the Pt band, from many large particles to fewer and smaller particles, with increasing distance from the cathode, a common observation for Pt bands in OCV hold tested membranes [34,44,45,54,56].

On the other hand, the number of particles per area in the baseline was at least one order of magnitude higher than in the ceria-containing MEAs. The combination of more but smaller particles means that the total area covered by the particles in the baseline was at least three times as high, demonstrating that less Pt has been deposited in the ceria-containing MEAs.

The plot of particle sizes versus the normalized distance from the cathode, shown in Fig. 4, supports the previous numerical

Table 2
Pt band average particle diameter, relative particle counts and area coverage.

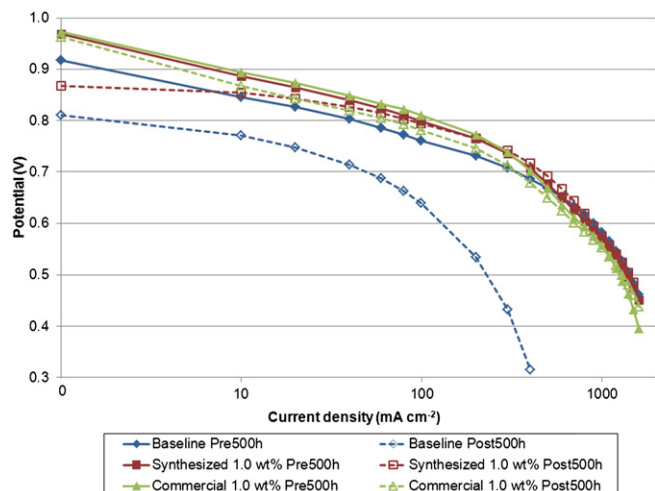|	Baseline	Synthesized		Commercial	
		1.0 wt%	2.0 wt%	1.0 wt%	2.0 wt%
Average diameter(nm)	19.0 ± 10.1	31.9 ± 26.8	71.3 ± 51.6	50.1 ± 30.1	35.3 ± 21.7
Particle counts per μm²	253	8	2	1	24
Area coverage	9.3%	1.8%	1.3%	0.7%	3.2%

Fig. 5. Pre- and post 500 h test performance curves.

observations. The basic shape of the particle size-distance distribution is similar for all MEAs. The black line in Fig. 4 indicates the theoretical distance of the Pt band from the cathode, calculated according to references [57] and [58] as a function of hydrogen and oxygen partial pressures. With increasing distance from the cathode, the particles decreased in both size and number. For the ceria-containing MEAs, the Pt particles were noticeably larger and the band extended much further into the membrane than for the baseline MEA. It should be noted that very small Pt particles (<3 nm), observed in some cases beyond the Pt band and, to a lesser extent, between the cathode and onset of the Pt band, were not included in the measurements.

Currently it is thought that the nanoparticles are formed by the reduction of diffusing Pt ions by H_2 crossing over from the anode.

Due to the crossover of both hydrogen and oxygen, a potential profile for an MEA in a running fuel cell is present, which has been modeled as a function of partial gas concentrations. Deposition mainly occurs at the point where the potential rapidly decreases to 0 V, resulting in the formation of the intense band, though particles do form further in the membrane, due to inhomogeneities in the gas crossover and the presence of seeding points [54,56–58].

The decrease in the number of particles in the Pt bands of ceria-containing membranes demonstrates that ceria influences the behavior of dissolved Pt ions. As all MEAs showed a similar decrease in ECA, it is unlikely that ceria prevents catalyst dissolution. The observation that particles extend further into the membrane, sometimes even all the way to the anode, suggests that the presence of ceria changes the potential profile. Brooker et al. [59] has shown that the inclusion of redox-active heteropolyacids in a sub-layer between the catalyst and the membrane, perturbs the potential profile resulting in the deposition of the metal in said sublayer. It is proposed here that a similar mechanism is at play. It is considered that the ceria particles, to some extent, influence the point at which the potential decreases to 0 V, thereby broadening the band.

It is difficult to ascertain whether the change in the Pt band affects membrane degradation in a positive or negative manner. Radicals can form on platinum from reactions of hydrogen and oxygen. On large particles these radicals are more likely to be quenched before escaping the surface than on smaller particles [54]. This suggests that in ceria-containing MEAs where larger, and fewer, particles were present, the Pt band contributes less to degradation than in the baseline. However, more research in this area is required, especially with regard to interparticle distance and change in the potential profile due to ceria presence.

3.1.4. Side-product analysis

During the IC analysis, other ions were observed in some of the baseline MEA effluents. In addition to fluoride, sulfate, a typical fuel
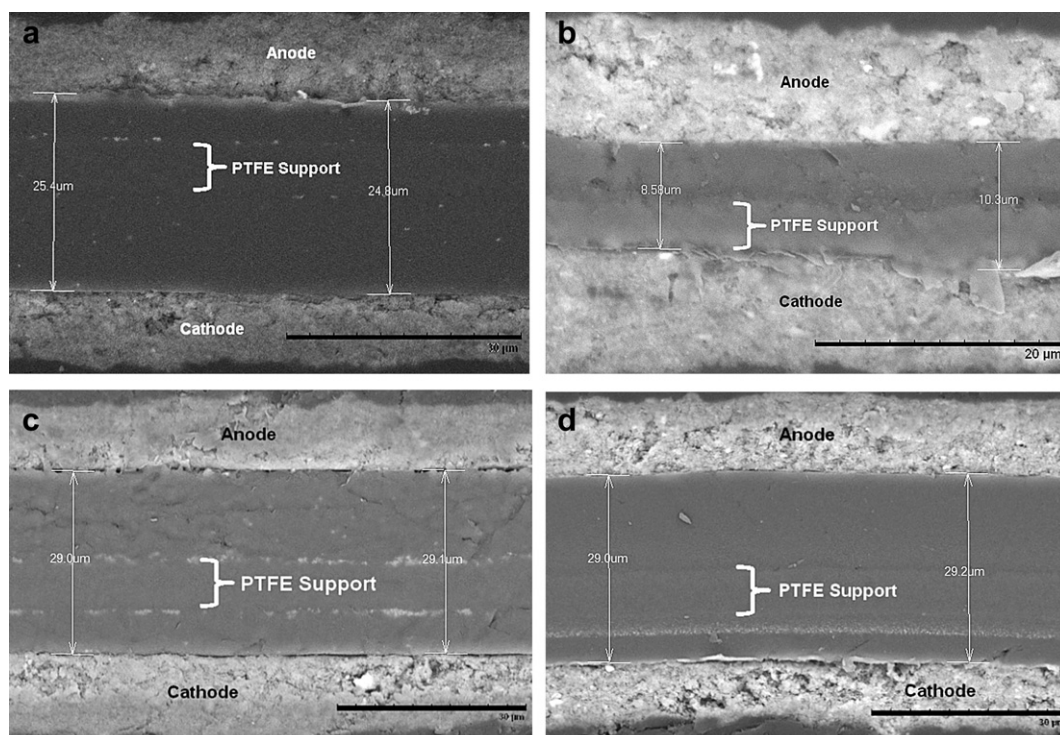

Fig. 6. SEM images of CCM cross-sections: baseline a) before and b) after 500 h OCV hold test; commercial 1.0 wt% ceria c) before and d) after 500 h OCV hold test.

Table 3
Total emission of fluoride, hydrogen crossover, OCV decay rate and resistance change for 500 h test.

	Baseline	Synthesized 1.0 wt%	Commercial 1.0 wt%
Total fluoride emission (μmol)	3800	340	33
Membrane fluorine inventory loss	89%	8%	0.9%
Pre500 h H_2 crossover & shorting current density (mA cm^{-2})	0.73	0.93	1.00
Post500 h H_2 crossover & shorting current density (mA cm^{-2})	21.49	10.04	0.80
OCV decay rate (mV h^{-1})	0.847	0.363	0.120
OCV decay rate (mV h^{-1}) until pinhole formation		0.151	0.116
Pre500 h resistance @ 400 mA cm^{-2} (mΩ cm)	67	72	78
Post500 h resistance @ 400 mA cm^{-2} (mΩ cm)	469	70	85

cell degradation compound [1], and chloride, an impurity, were identified. Moreover, two unknown peaks were seen. Due to low concentrations, the molecule associated with only one of the peaks could be identified as trifluoroacetic acid (TFA). The TFA concentrations were found to mirror the emission of fluoride, which is in line with conclusions reached by Chen and Fuller who described a mechanism of side-chain degradation that results in TFA formation [4]. The MEAs containing ceria did not show any TFA formation, demonstrating that the additive is effective at reducing all radical attack.

3.2. 500 h OCV hold durability testing

The 94 h OCV hold tests showed a large reduction in the amount of fluoride released and the OCV decay rate as a consequence of the addition of cerium oxide to the membranes. However, the time frame was too short to determine any significant impact on either membrane thickness, hydrogen crossover or performance. To ascertain cerium oxide's radical scavenging ability over longer periods of time, 500 h OCV hold tests were performed on a baseline, a synthesized 1.0 wt% and commercial 1.0 wt% MEA. The test conditions, shown in Table 1, were based on DOE specifications [1], which involved higher flow rates than the 94 h OCV experiment, and were performed under pressure to increase gas crossover and, thereby, accelerate degradation.

The pre-test hydrogen crossover, platinum ECA and performance (Fig. 5) were found to be comparable to the 94 h tested MEAs.

One issue encountered during testing was that the synthesized 1.0 wt% MEA developed a defect after ca. 350 h, which lead to a very large increase in hydrogen crossover. As explained below, the nature of the defect was determined to be localized, as opposed to a general failure of the MEA.

The baseline cell degraded severely, losing over half of its total fluorine content during the first 100 h of measurement. The MEA remained intact by virtue of the structural integrity provided by the PTFE support. The SEM images in Fig. 6a and b show that the membrane thinned considerably, from ∼25 μm to 8–10 μm, whereby the membrane on the cathode side was completely degraded, leaving the PTFE support in direct contact with the electrode. One consequence of the membrane thinning was the development of an electrical short, most likely due to the penetration of carbon fibers through the membrane, which influenced the linear sweep voltammetry measurements. The 25/25/25 LSV data given in Table 3 for the baseline MEA includes the decreased resistance due to the short and though it does not present accurate values for the hydrogen crossover, it clearly shows increased gas permeability. This is further supported by IR images that the MEA developed pinholes, which are visible as intense red spots in Fig. 7a.

The addition of ceria had a significant influence on the degradation, reducing the total amount of fluoride released by one to two orders of magnitude (Table 3). However, such simple comparisons are not adequate. Literature observations of the FER indicate that it generally increases during fuel cell testing [44,45], which was observed for both ceria-containing MEAs (Fig. 8). The baseline cell however, as mentioned, lost the majority of its fluoride within the first 100 h. As shown in Fig. 8, its FER actually decreased with little further degradation occurring after ∼150 h, due to the lack of membrane to degrade. If more membrane had been available, it is safe to assume that the baseline MEA's total emission of fluoride would have been much greater.

The fluoride emission of the first 140 h for the synthesized ceria 1.0 wt% and 400 h for the commercial ceria 1.0 wt% MEAs were below the limit of quantification, a substantial improvement over the baseline material. Based on the LOQ, the FER of the ceria-containing MEAs was two orders of magnitude lower, values in line with those obtained for cerium ion-exchange [1,5]. Surprisingly, the defect in the synthesized 1.0 wt% MEA did not impact the FER (Fig. 8). Prior to the pinhole formation, which is shown in Fig. 7b as an intense red area of higher temperature; it had already released approximately half of the total fluoride measured during the experiment (Fig. 8). This failure was, therefore, considered to be localized and not representative of the whole membrane. The amount of fluoride released was still one order of magnitude lower than the baseline. Throughout the 500 h of the experiment, the commercial 1.0 wt% MEA lost less than one percent of its total fluorine inventory (Table 3) and showed no change in membrane
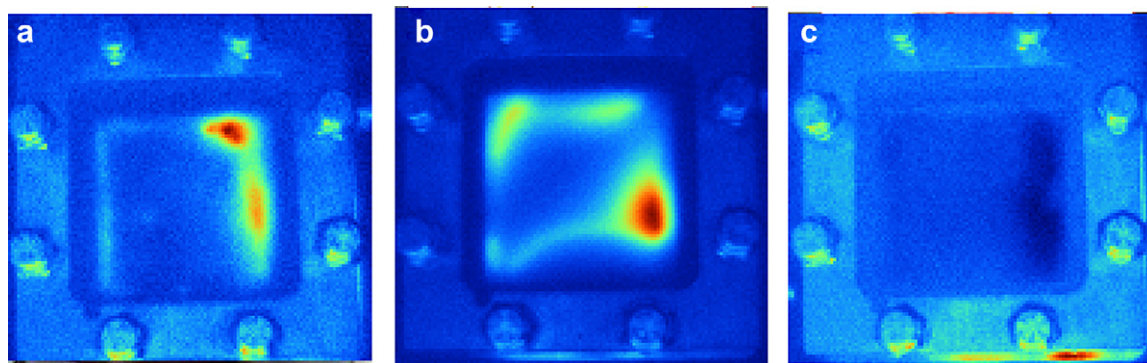

Fig. 7. IR images of CCMs after 500 h OCV hold test: a) Baseline, b) synthesized 1.0 wt% h and c) commercial ceria 1.0 wt% (red areas (darker areas within the lighter areas in the black and white images) show higher temperature caused by reaction of hydrogen and air due to hydrogen crossover). (For interpretation of the references to colour in this figure legend, the reader is referred to the web version of this article.)
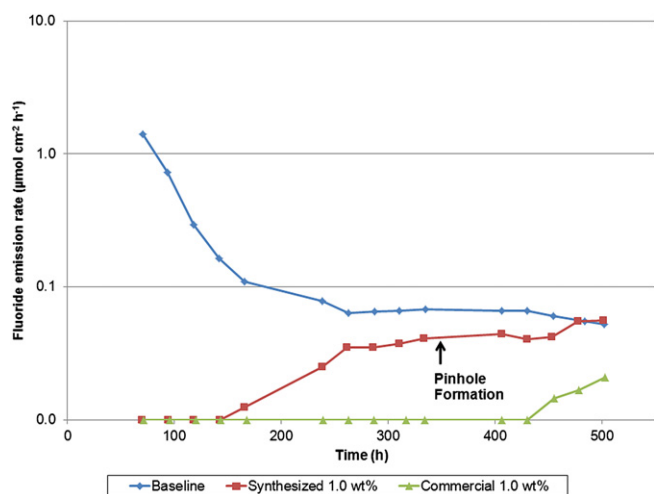
Fig. 8. Fluoride emission rates for the 500 h OCV hold test.

thickness (Fig. 6c and d). IR images, a representative sample is given in Fig. 7c, showed no significant hydrogen crossover.

Though it did not impact the emission of fluoride, the defect formation in the synthesized 1.0 wt% MEA did increase the OCV decay rate that, until 350 h, had been similar to the commercial 1.0 wt%. The values measured and given in Table 3, ~ 0.1 mV h^{-1}, are in line with literature data [6]. In Fig. 9, the sudden decrease in potential after the pinhole formation can be seen, which correlates well with the rapid increase in hydrogen crossover observed in the daily LSV measurements.

The potential plot for the baseline MEA is also given in Fig. 9 and shows a very fast decay in the first ~ 40 h due to the large degradation which slows, presumably due the membrane compacting. The overall OCV decay rate was seven times higher than for the ceria-containing MEAs (Table 3).

The membrane degradation had a very large effect on the both the performance (Fig. 5) and resistance, which increased seven-fold (Table 3), of the baseline MEA. The performance, which pre-test had shown to be very similar to the ceria-containing MEAs; decreased dramatically and did not even pass 400 mA cm^{-2}. The fact that any performance could be measured was once again due to the PTFE support. The pinhole in the synthesized 1.0 wt% MEA only affected

its performance in the low current density regions (<20 mA cm^{-2}) where the hydrogen crossover has a significant impact on the potential. At higher currents, both ceria-containing MEAs were unchanged with regard to their pre-test performance. The commercial 1.0 wt% MEA showed a slight increase in resistance, which is considered to be within the error of the experiment. Otherwise, no significant change in any parameters that would indicate a lowering in proton conductivity was measured. While this provides little reason to believe that cerium oxide is being reduced to Ce^{3+}, more work in this area is needed.

When comparing the 94 h and 500 h tests, it is clear that the shorter test is insufficient in demonstrating the very large durability improvement that ceria provides fuel cell membranes. The decrease in the total emission of fluoride upon incorporation of the additives for the 500 h test was more than an order of magnitude larger than the 94 h test showed. Barring localized failures, ceria, of either formulation, was able to dramatically inhibit membrane degradation, to the extent that even after 500 h of extreme degradation conditions, membrane electrode assemblies remain nearly pristine.

4. Conclusion

Two formulations of crystalline cerium oxide nanoparticles of varying particle sizes, an in-house synthesized and a commercially available material, were incorporated into PTFE-supported composite perfluorosulfonic acid hydrogen fuel cell membranes and coated with a platinum on carbon catalyst. These MEAs were held at OCV with hydrogen and air for 94 and 500 h. Pre- and post-test performance and hydrogen crossover were determined and OCV decay and fluoride emission were monitored throughout the experiments.

The 94 h test confirmed the findings in shorter tests that cerium oxide acts as a radical scavenger and protects the membrane. This reduced both the OCV decay and fluoride emissions dramatically, independent of concentration and particle size. The analysis of the platinum particles observed in the membrane showed that Pt band formation is also influenced by the presence of this additive. Cerium oxide incorporation resulted in the formation of fewer and larger particles, reaching further into the membrane with less platinum precipitation overall. It is suggested that the potential profile through the membrane is perturbed by the presence of the ceria, resulting in an altered Pt band.

In 500 h tests, a baseline MEA degraded severely, losing nearly 90% of its fluorine inventory with a concomitant two- to threefold decrease in thickness. This lead to the development of a short, a large increase in hydrogen crossover, consequent high OCV decay, and a large performance deterioration. The MEA survived the test only due to the presence of its PTFE support. Incorporation of ceria reduced the OCV decay rate and fluoride emission dramatically. An in-house synthesized ceria MEA developed a localized pinhole, which impacted its hydrogen crossover and low current performance. Addition of 1.0 wt% of the commercial ceria resulted in sevenfold decrease in the OCV decay rate versus the baseline while losing less than 1% of its fluorine inventory. It also showed no change in performance and hydrogen crossover, resulting in an essentially unchanged MEA that seems capable of showing the required durability for practical applications.

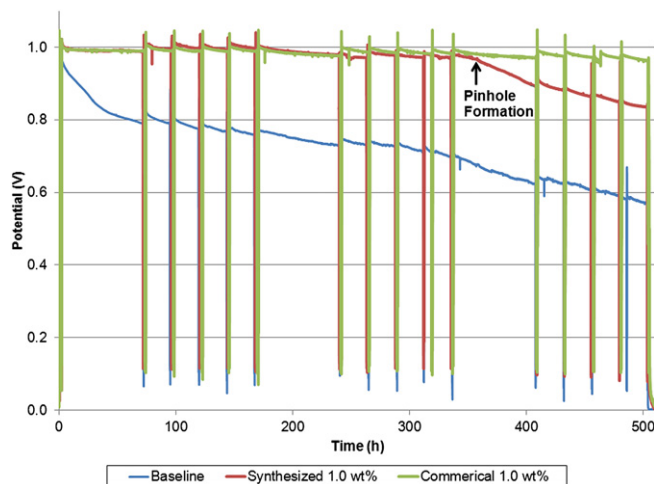**Fig. 9.** OCV decay for 500 h OCV hold (spikes in potential show breaks in the experiment to perform electrochemical measurements).

References

[1] M.M. Mench, E.C. Kumbur, T.N. Veziroglu (Eds.), Polymer Electrolyte Fuel Cell Degradation, first ed., Elsevier Ltd., 2012.
[2] Y. Luan, Y. Zhang, PEM Fuel Cell Failure Mode Analysis, CRC Press, 2012, pp. 73—108.
[3] T. Xie, C.A. Hayden, Polymer 48 (2007) 5497—5506.
[4] C. Chen, T.F. Fuller, Polym. Degrad. Stab. 94 (2009) 1436—1447.
[5] F.D. Coms, ECS Trans. 16 (2008).
[6] S. Xiao, H. Zhang, C. Bi, Y. Zhang, Y. Zhang, H. Dai, Z. Mai, X. Li, J. Power Sources 195 (2010) 5305—5311.
[7] S. Xiao, H. Zhang, X. Li, Z. Mai, Int. J. Hydrogen Energy 36 (2011) 10934—10939.
[8] S. Kundu, M. Fowler, L.C. Simon, R. Abouatallah, J. Power Sources 182 (2008) 254—258.
[9] H. Wang, H. Li, X.-Z. Yuan (Eds.), PEM Fuel Cell Failure Mode Analysis, CRC Press, 2012.
[10] D.E. Curtin, R.D. Lousenberg, T.J. Henry, P.C. Tangeman, M.E. Tisack, J. Power Sources 131 (2004) 41—48.
[11] T.R. Ralph, D.E. Barnwell, P.J. Bouwman, A.J. Hodgkinson, M.I. Petch, M. Pollington, J. Electrochem. Soc. 155 (2008) B411.
[12] G.M. Haugen, F. Meng, N. Aieta, J.L. Horan, M.-C. Kuo, M.H. Frey, S.J. Hamrock, A.M. Herring, ECS Trans. 3 (2006) 551—559.
[13] M.A. Navarra, C. Abbati, B. Scrosati, J. Power Sources 183 (2008) 109—113.
[14] K.T. Park, U.H. Jung, D.W. Choi, K. Chun, H.M. Lee, S.H. Kim, J. Power Sources 177 (2008) 247—253.
[15] Y. Patil, S. Kulkarni, K.A. Mauritz, J. Appl. Polym. Sci. (2011). n/a—n/a.
[16] Y. Patil, S. Sambandam, V. Ramani, K. Mauritz, J. Electrochem. Soc. 156 (2009) B1092—B1098.
[17] P. Trogadas, V. Ramani, J. Power Sources 174 (2007) 159—163.
[18] P. Trogadas, V. Ramani, J. Electrochem. Soc. 155 (2008) B696—B703.
[19] N.R. de Tacconi, C.R. Chenthamarakshan, K. Rajeshwar, W.-Y. Lin, T.F. Carlson, L. Nikiel, W.A. Wampler, S. Sambandam, V. Ramani, J. Electrochem. Soc. 155 (2008) B1102—B1109.
[20] S. Xiao, H. Zhang, C. Bi, Y. Zhang, Y. Ma, X. Li, H. Zhong, Y. Zhang, J. Power Sources 195 (2010) 8000—8005.
[21] M. Aoki, H. Uchida, M. Watanabe, Electrochem. Commun. 7 (2005) 1434—1438.
[22] V. Ramani, P. Trogadas, S. Sambandam, Abstracts of Papers, 238th ACS National Meeting, Washington, DC, United States, August 16—20, 2009, FUEL-183.
[23] P. Trogadas, Department of Chemical and Biological Engineering, Illinois Institute of Technology, Illinois, 2009.
[24] P. Trogadas, J. Parrondo, F. Mijangos, V. Ramani, J. Mater. Chem. 21 (2011) 19381.
[25] P. Trogadas, J. Parrondo, V. Ramani, Electrochem. Solid State Lett. 11 (2008) B113—B116.
[26] P. Trogadas, J. Parrondo, V. Ramani, Abstracts of Papers, 238th ACS National Meeting, Washington, DC, United States, August 16—20, 2009, PMSE-100.
[27] P. Trogadas, J. Parrondo, V. Ramani, Degradation mitigation in PEM fuel cells using metal nanoparticle and metal oxide additives, in: Functional Polymer Nanocomposites for Energy Storage and Conversion, American Chemical Society, 2010, pp. 187—207.
[28] P. Trogadas, J. Parrondo, V. Ramani, PMSE Preprints 100 (2009) 459—460.
[29] P. Trogadas, J. Parrondo, V. Ramani, Chem. Commun. 47 (2011) 11549.
[30] P. Trogadas, V. Ramani, ECS Trans. 25 (2009) 443—451.
[31] P. Trogadas, V.K. Ramani, PMSE Preprints (2010).
[32] E. Endoh, ECS Trans. 16 (2008) 1229—1240.
[33] D. Zhao, B.L. Yi, H.M. Zhang, H.M. Yu, L. Wang, Y.W. Ma, D.M. Xing, J. Power Sources 190 (2009) 301—306.
[34] F.D. Coms, H. Liu, J.E. Owejan, ECS Trans. 16 (2008) 1735—1747.
[35] A. Karakoti, Mechanical, Materials and Aerospace Engineering, University of Central Florida, Orlando, 2010.
[36] A. Karakoti, S. Singh, J.M. Dowding, S. Seal, W.T. Self, Chem. Soc. Rev. 39 (2010) 4422—4432.
[37] A.S. Karakoti, S.V.N.T. Kuchibhatla, K.S. Babu, S. Seal, J. Phys. Chem. C 111 (2007) 17232—17240.
[38] A.S. Karakoti, N.A. Monteiro-Riviere, R. Aggarwal, J.P. Davis, R.J. Narayan, W.T. Self, J. McGinnis, S. Seal, JOM 60 (2008) 33—37.
[39] A.S. Karakoti, S. Singh, A. Kumar, M. Malinska, S.V.N.T. Kuchibhatla, K. Wozniak, W.T. Self, S. Seal, J. Am. Chem. Soc. 131 (2009) 14144—14145.
[40] K. Yasuda, A. Taniguchi, T. Akita, T. Ioroi, Z. Siroma, Phys. Chem. Chem. Phys. PCCP 8 (2006) 746—752.
[41] C.G. Chung, L. Kim, Y.W. Sung, J. Lee, J.S. Chung, Int. J. Hydrogen Energy 34 (2009) 8.
[42] L. Kim, C.G. Chung, Y.W. Sung, J.S. Chung, J. Power Sources 183 (2008) 9.
[43] T. Akita, A. Taniguchi, J. Maekawa, Z. Siroma, K. Tanaka, M. Kohyama, K. Yasuda, J. Power Sources 159 (2006) 7.
[44] N.E. Cipollini, Mater. Res. Soc. Symp. Proc. 885 (2006) 33—44.
[45] N.E. Cipollini, ECS Trans. 11 (2007) 1071—1082.
[46] W. Yoon, X. Huang, J. Electrochem. Soc. 157 (2010) B599—B606.
[47] J. Peron, D.J. Jones, J. Roziere, ECS Trans. 11 (2007) 7.
[48] W. Bi, G.E. Gray, T.F. Fuller, Electrochem. Solid State Lett. 10 (2007) B101.
[49] J. Zhang, B.A. Litteer, W. Gu, H. Liu, H.A. Gasteiger, J. Electrochem. Soc. 154 (2007) B1006.
[50] W. Yoon, X. Huang, J. Electrochem. Soc. 157 (2010) B680.
[51] L. Gubler, S.M. Dockheer, W.H. Koppenol, J. Electrochem. Soc. 158 (2011) B755.
[52] M.P. Rodgers, N. Mohajeri, L.J. Bonville, D.K. Slattery, J. Electrochem. Soc. 159 (2012) B564.
[53] E. Endoh, S. Hommura, S. Terazono, H. Widjaja, J. Anzai, ECS Trans. 11 (2007) 1083—1091.
[54] M. Gummalla, V. Atrazhev, D. Condit, N. Cipollini, T. Madden, N.Y. Kuzminyh, D. Weiss, S. Burlatsky, J. Electrochem. Soc. 157 (2010) B1006.
[55] P.J. Ferreira, Y. Shao-Horn, Electrochem. Solid State Lett. 10 (2007) 4.
[56] S.F. Burlatsky, V. Atrazhev, N. Cipollini, D. Condit, N. Erikhman, ECS Trans. 1 (2006) 239—246.
[57] V.V. Atrazhev, N.S. Erikhman, S.F. Burlatsky, J. Electroanal. Chem. 601 (2007) 251—259.
[58] R.M. Darling, J.P. Meyers, J. Electrochem. Soc. 150 (2003) A1523.
[59] R.P. Brooker, L.J. Bonville, D.K. Slattery, J. Electrochem. Soc., in press.